First-principles study of the electronic, vibrational, electron–phonon interaction and thermodynamics properties of $ZrNi_2Ga$

2009 J. Phys.: Condens. Matter 21 075501

(http://iopscience.iop.org/0953-8984/21/7/075501)

J. Phys.: Condens. Matter **21** (2009) 075501 (7pp) doi:10.1088/0953-8984/21/7/075501

First-principles study of the electronic, vibrational, electron–phonon interaction and thermodynamics properties of $ZrNi_2Ga$

Wenmei Ming, Yi Liu, Wei Zhang, Jianzhi Zhao and Yugui Yao

Beijing National Laboratory for Condensed Matter Physics, and Institute of Physics, Chinese Academy of Sciences, Beijing 100190, People's Republic of China

E-mail: ygyao@aphy.iphy.ac.cn

Received 24 November 2008, in final form 22 December 2008
Published 23 January 2009
Online at stacks.iop.org/JPhysCM/21/075501

Abstract

Using first-principles calculation, we investigate systematically the properties of $ZrNi_2Ga$ with fcc $L2_1$ Heusler structure, including the electronic structure, phonon dispersion, electron–phonon interaction and thermodynamics. The calculated electron–phonon coupling constant λ and the logarithmically averaged frequency $\langle\omega\rangle_{\log}$ are 0.747 and 68.48 cm^{-1}, respectively, giving the superconducting transition temperature $T_c = 3.15$ K according to the Allen–Dynes formula. It is in good agreement with the corresponding experimental T_c and $ZrNi_2Ga$ therefore can be explained as a conventional phonon-mediated superconductor.

(Some figures in this article are in colour only in the electronic version)

1. Introduction

The Heusler structure with formula AB_2Z (A and B are transition metals, Z is an sp element) is considered to be one of the prototypes of half-metallic ferromagnets (HFM) [1, 2]. It has attracted much attention from both experimental and theoretical communities in the past decades, since HFM are characterized by possessing unit spin polarization ($P = 1$) due to the fact that they are metallic for one spin and semiconducting for another spin. It has promising uses in spintronics [3, 4]. Meanwhile, a few Heusler structure compounds containing rare earth metals (i.e. A is a rare earth atom) [5–11] exhibit either magnetic order (for instance, RPd_2Sn with R = Tb, Dy, Ho) or superconductivity (RPd_2Sn with R = Tm, Lu) with T_c less than 3.5 K. Also, the coexistence of superconductivity and magnetism was found in $YbPd_2Sn$ [6] and $ErPd_2Sn$ [7]. It was generally believed that the magnetism originated from the rare earth sublattice and superconductivity came from the transition-metal sublattice for this class of compounds [9]. However, exchange interaction between f-electrons of the rare earth and d-electrons of the transition atom could have a dramatic influence on superconductivity. A large exchange interaction would suppress the superconductivity and a small exchange interaction might give rise to the coexistence of superconductivity and magnetic order [10]. Superconductivity was also found in similar compounds with A replaced by a transition-metal atom, such as YPd_2Sn [12], $NbNi_2Sn$ [13], $NbNi_2Al$ [14], $ZrPd_2Al$ and $HfPd_2Al$ [15] with the highest T_c of 4.9 K in YPd_2Sn. It was pointed out that the superconductivity of $ZrPd_2Al$ and $HfPd_2Al$ could be understood by the valence instability at the L point due to a Van Hove singularity (VHS) [15].

Recently Winterlik *et al* reported a new rich-in-Ni Heusler superconductor $ZrNi_2Ga$ [16] with T_c about 2.9 K. Their measurements showed that this compound was in the paramagnetic state at low temperature. It was the same as the situation in $NbNi_2Sn$, $NbNi_2Al$, $ZrPd_2Al$ and $HfPd_2Al$. Understanding the superconducting mechanism of a new superconductor is always full of interest. Theoretical calculations of electronic structure, phonon structure and electron–phonon interaction can serve as useful tools for us to gain a preliminary insight into the superconductivity. Therefore, in this work we start from first-principles calculation to get the superconducting mechanism of $ZrNi_2Ga$ and to obtain a complete knowledge of the static

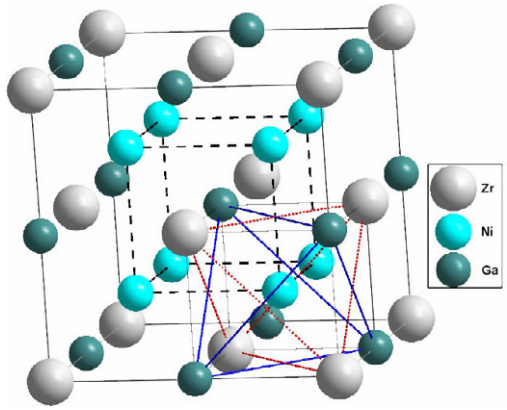

Figure 1. The fcc $L2_1$ Heusler structure of $ZrNi_2Ga$: the dotted and solid lines highlight the Zr tetrahedron and Ga tetrahedron, respectively, and the dashed lines highlight the cubic coordinates of Ni.

electron-related and dynamic phonon-related properties of this superconductor in its normal state.

This paper is organized as follows: the detailed computational method is described in section 2, the results and discussion of electronic structure, phonon structure as well as electron–phonon interaction and thermodynamics properties are given in section 3 and the conclusion is made in section 4.

2. Computational details

Our calculations are performed with density functional theory (DFT) [17] and density functional perturbation theory (DFPT) [18] for an accurate electronic structure and phonon dispersion relationship, respectively. The full potential linearized augmented plane wave (FP-LAPW) method within the WIEN2K package [19] is used for electronic structure calculation with a plane wave cutoff $R_{\mathrm{MT}}K_{\max} = 8.5$, muffin-tin radii of 2.43 bohr, 2.43 bohr and 2.28 bohr for Zr, Ni and Ga, respectively, and basis expansion up to $l = 10$. A $12\times12\times12$ k-mesh is used for Brillouin zone integration with a modified tetrahedron method [20] to guarantee the convergence of total energy. For phonon dispersion and electron–phonon interaction calculation, the plane wave pseudopotential method implemented in the PWSCF package [21] is used and optimized norm-conversing pseudopotentials [22] generated from the OPIUM package [23] are adopted. The energy cutoff is set to be 60 Ryd for the expansion of the electronic wavefunction. A $12 \times 12 \times 12$ k-mesh is used for Brillouin zone integration to obtain the ground state and a $36\times36\times36$ k-mesh is used for double δ function integration in the Eliashberg function calculation (see section 3.4) [24, 25], along with a Methfessel–Paxton Gauss smearing [26] of 0.02 Ryd. A $4 \times 4 \times 4$ q-mesh is used to compute the dynamical matrix and then a Fourier interpolation is employed to obtain phonon frequencies in the full Brillouin zone. For comparison, both the local density approximation (LDA) and the generalized gradient approximation (GGA) are employed to approximate the exchange–correlation potential.

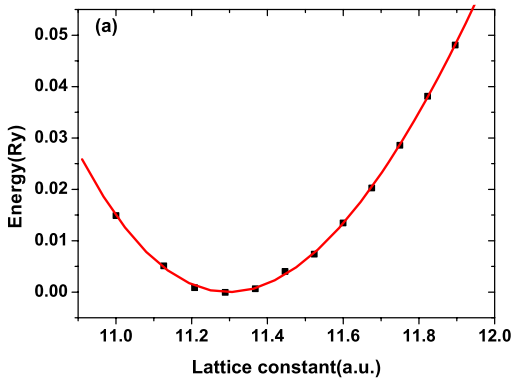

Figure 2. The calculated LDA equation of states for $ZrNi_2Ga$.

Table 1. Calculated lattice parameter a_0 (au) and bulk modulus B_0 (kbar). The experiment lattice constant (Exp.) is also given for comparison.

	WIEN2K		PWSCF		
	LDA	GGA	LDA	GGA	Exp.
a_0	11.295	11.560	11.441	11.707	11.524
B_0	1817	1535	1815	1496	

3. Results and discussion

3.1. Structure properties

$ZrNi_2Ga$ crystallizes in an fcc $L2_1$ Heusler structure (of $Fm\bar{3}m$ symmetry) depicted in figure 1. Zr atoms, Ga atoms and Ni atoms occupy the 4a(0, 0, 0), 4b($\frac{1}{2}$, $\frac{1}{2}$, $\frac{1}{2}$) and 8c($\frac{1}{4}$, $\frac{1}{4}$, $\frac{1}{4}$) Wyckoff positions, respectively. Both Ga atom and Zr atom are coordinated by eight Ni atoms, every Ni atom is surrounded by four Zr atoms in the Zr tetrahedron and four Ga atoms in the Ga tetrahedron. The theoretical equilibrium lattice parameter a_0 and bulk modulus B_0 are summarized in table 1. In figure 2, we present the calculated LDA equation of states of $ZrNi_2Ga$ with the WIEN2K package. The equilibrium lattice parameter and bulk modulus are obtained by fitting the total energy versus lattice constant points to a Murnaghan-state equation [27]. The optimized lattice parameter from GGA is slightly larger than the experimental lattice parameter, while the corresponding lattice parameter from LDA is slightly smaller than the experimental lattice parameter, both of which are typical behaviors in DFT calculations. In the following sections, all our results are presented for the theoretical equilibrium geometry from LDA.

3.2. Electronic structure

To have an explicit understanding of the interaction among different orbitals of atoms, we first show the total and projected density of states (DOS) of $ZrNi_2Ga$ in figure 3.[1] Obviously, contributions to DOS from -4 to 4 eV are mainly from Zr

[1] Electronic structure from PWSCF is very close to that from WIEN2K, which demonstrates that the pseudopotentials used in our work are accurate and have satisfactory transferability. Here we thus only show the electronic structure from WIEN2K.

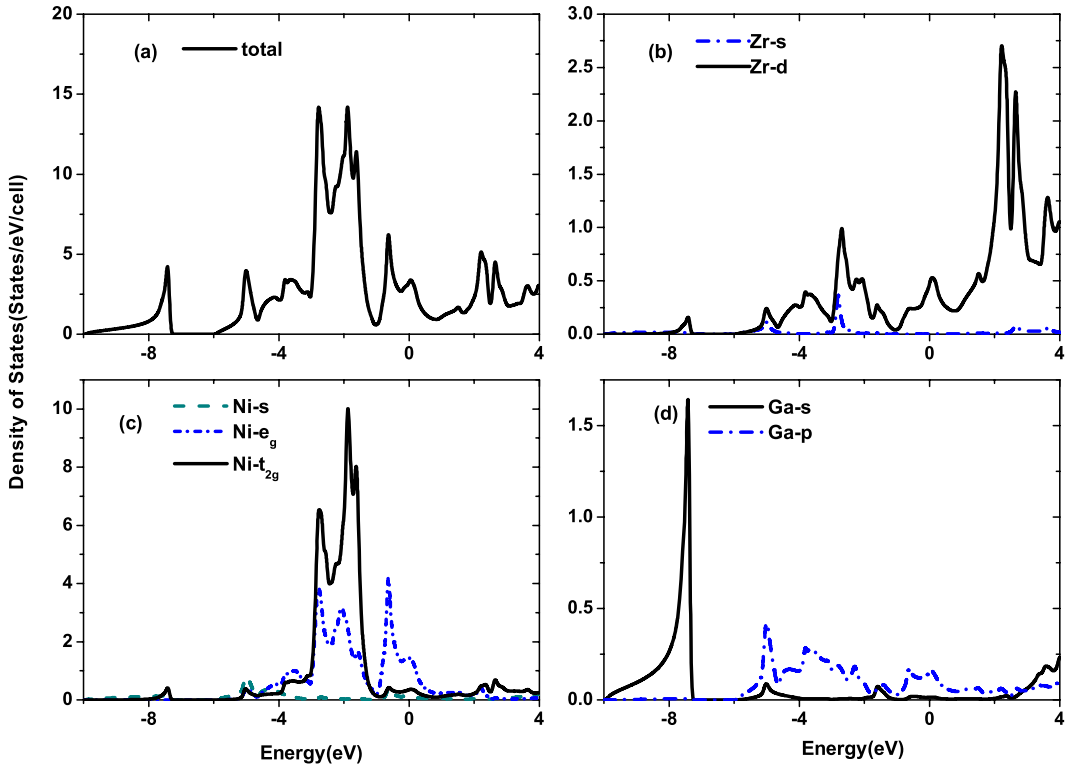

Figure 3. The calculated LDA total and projected electron density of states (Fermi level is located at energy = 0 eV).

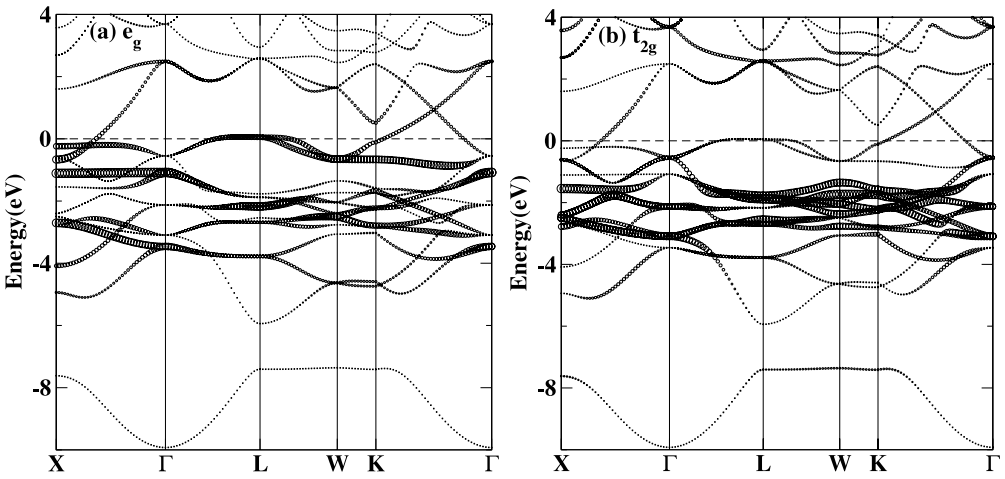

Figure 4. The calculated band structures with projection to (a) Ni-e_g states and to (b) Ni-t_{2g} states, shown by fat bands (Fermi level is located at energy = 0 eV).

3d states and Ni 3d states, but other terms are much smaller. In this energy range the Ni-e_g states and the Ni-t_{2g} states are not separated from each other as expected, but instead they have significant overlap and there are more e_g states above the Fermi energy. Usually an undistorted tetrahedron crystal field splits five degenerated d-orbitals into low-lying twofold e_g states and up-lying threefold t_{2g} states. However, in $ZrNi_2Ga$ every Ni atom is surrounded by two sets of tetrahedra occupied by Zr atoms and Ga atoms, respectively, as mentioned in section 3.1. Therefore the splitting effects on Ni 3d orbitals are intertwined, which are naturally different from traditional predictions. The Fermi energy (DOS at Fermi energy is 3.25 states/cell/eV) is located very near to a VHS. This may result in a probable Stoner instability, which might bring the system to be ferromagnetic, but our calculation has verified that an initial magnetic calculation will eventually converge to the non-magnetic ground state. In addition, between −7.3 and −6.0 eV there exists a gap which is believed to be a typical behavior of Heusler compounds [15].

In figure 4, we show the calculated band structure along several high symmetry directions. Narrow bands with projections to Ni-e_g states and Ni-t_{2g} states in figures 4(a) and (b) demonstrate clearly that the Ni d-orbital splitting is very complicated, different from the result induced by a simple

Table 2. Comparison of the frequencies (cm^{-1}) at X and Γ with LDA and GGA.

X	$E_u(1)$	$A_{2u}(1)$	B_{1u}	$E_u(2)$	E_g	A_{1g}	$A_{2u}(2)$	E_u
LDA	74.9	129.4	140.0	142.3	145.2	156.7	223.4	229.6
GGA	75.5	125.8	135.5	137.4	140.0	153.3	209.6	216.9
Γ		$T_{1u}(1)$		T_{2g}		$T_{1u}(2)$		$T_{1u}(3)$
LDA		0.0		92.8		185.9		215.9
GGA		0.0		95.5		178.5		204.2

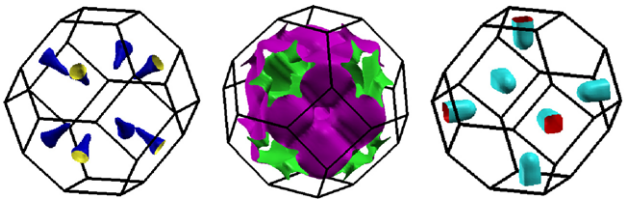

Figure 5. The calculated Fermi surfaces (FSs) of $ZrNi_2Ga$.

tetrahedron crystal field. At the same time, there are three bands cutting across the Fermi energy: two of them show almost no dispersion around the L point, where the band energy stays above but quite close to the Fermi energy, resulting in a VHS near the Fermi energy as discussed above.

The topology of a Fermi surface (FS) is an important factor to evaluate the mechanism of superconductivity and transport properties of metallic systems, in both of which phonon-mediated scattering of electrons may play an important role. Moreover, the electron–phonon interaction is usually very sensitive to the shape of FS [24, 25, 28]. Therefore, we next show the calculated FSs of $ZrNi_2Ga$ in figure 5. The FSs consist of three parts, corresponding to the three bands (as shown in figure 4) crossing the Fermi energy.

3.3. Phonon dispersion

In this section, we focus on its vibrational properties at the equilibrium lattice of 11.441 au within LDA. The phonon band structure and the corresponding phonon density of states (PHDOS) are obtained, as shown in figures 6 and 7, respectively. There are 12 phonon branches in the full phonon dispersion since the unit cell consists of four atoms which give rise to three acoustic and nine optic phonon branches. The low-lying nine branches below 200 cm^{-1} are separated from the up-lying three branches by a gap of about 5 cm^{-1}. Also, all phonon modes exhibit positive frequencies, strongly suggesting that the optimized $ZrNi_2Ga$ lattice is dynamically stable. We can therefore expect that at the optimized geometry $ZrNi_2Ga$ lies at least in its local minimum of energy. For comparison, we also carry out the calculation of the phonon band structure with GGA at the corresponding optimized lattice constant 11.707 au. The frequencies calculated from LDA and GGA are summarized in table 2 for X and Γ. In figure 7, we show both the total and atom-projected phonon DOS. The main contribution to phonon density states (below 160 cm^{-1}) comes from Ni vibrational modes. The contribution from Zr increases rapidly at higher energy (above 205 cm^{-1})

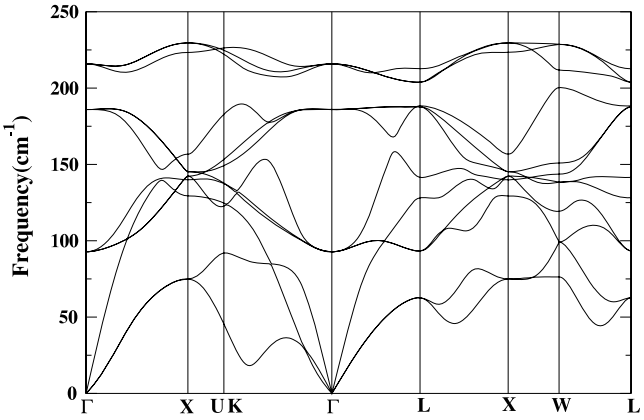

Figure 6. The calculated phonon dispersion of $ZrNi_2Ga$.

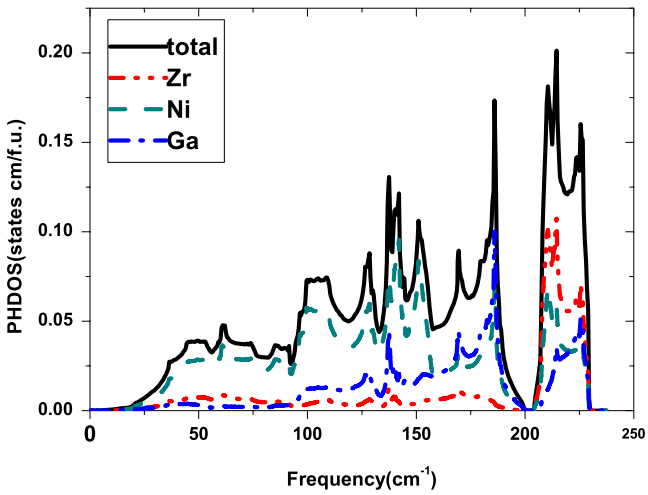

Figure 7. The calculated phonon total and atom-projected density of states of $ZrNi_2Ga$.

and is very small at lower energy (below 205 cm^{-1}) in spite of the heaviest mass of Zr in the three atom species. It can be naively expected that the strong vibrations of Ni may bring about strong electron–phonon interaction, which will be discussed in the following.

3.4. Electron–phonon interaction

After getting the electronic structure of $ZrNi_2Ga$ from static total energy calculations and dynamical lattice properties from DFPT, we will move onto the discussion of the interaction between electrons and phonons. The electron–phonon

coupling (EPC) constant (λ) is usually extracted from the Eliashberg function ($\alpha^2F(\omega)$) which can be used to determine the T_c of a conventional phonon-mediated superconductor. For clarity, these quantities are expressed as the following [25, 29]:

$$\alpha^2F(\omega) = \frac{1}{2\pi N(\varepsilon_F)} \sum_{q\nu} \frac{\gamma_{q\nu}}{\omega_{q\nu}} \delta(\omega - \omega_{q\nu}) \tag{1}$$

$$\gamma_{q\nu} = 2\pi\omega_{q\nu} \sum_{kjj'} |g^{q\nu}_{k+qj',kj}|^2 \delta(\varepsilon_{kj} - \varepsilon_F)\delta(\varepsilon_{k+qj'} - \varepsilon_F) \tag{2}$$

where $g^{q\nu,ij}_{k+q,k}$ is defined as

$$g^{q\nu,j'j}_{k+q,k} = \sum_{R,\nu} \frac{\eta_{q\nu}(R,\nu)}{\sqrt{2M_R\omega_{q\nu}}} \langle k+q, j'| \frac{\delta V_{\text{eff}}}{\delta R_\nu} |k, j\rangle. \tag{3}$$

The electron–phonon coupling constant λ is expressed in terms of the Eliashberg function:

$$\lambda = 2\int \frac{d\omega}{\omega}\alpha^2F(\omega) = \int d\omega\, \lambda(\omega). \tag{4}$$

Here, $\lambda(\omega) = \frac{2\alpha^2F(\omega)}{\omega}$.

From the calculated λ, T_c is estimated using the Allen–Dynes formula [30]:

$$T_c = \frac{\langle\omega\rangle_{\log}}{1.2} \exp\left[-\frac{1.04(1+\lambda)}{\lambda - \mu^*(1+0.62\lambda)}\right] \tag{5}$$

where the logarithmically averaged frequency $\langle\omega\rangle_{\log}$ is defined as

$$\langle\omega\rangle_{\log} = \exp\left[\frac{2}{\lambda}\int_0^{\omega_{\max}} \alpha^2F(\omega)\frac{\ln(\omega)}{\omega} d\omega\right]. \tag{6}$$

We show the calculated $\alpha^2F(\omega)$ in figure 8. The shape of $\alpha^2F(\omega)$ (on the left of figure 8(a)) exhibits remarkable variation (below 200 cm^{-1}) from that of PHDOS, while at high energy (above 200 cm^{-1}) the shape is already determined by the corresponding shape of PHDOS. This demonstrates that the phonon modes with lower energy (below 200 cm^{-1}) are more involved in the process of scattering of electrons than the phonon modes with higher energy. It is noteworthy that phonons with different energies almost make comparable contributions to $\alpha^2F(\omega)$. However, the situation of MgB_2 [31] is very different: there are only two narrow peaks in $\alpha^2F(\omega)$ predicting that only a few phonon modes have strong coupling with electrons while other modes gives much smaller contributions to the coupling. Mode resolved $\alpha^2F(\omega)$ in figure 8(b) further shows that at lower energy each mode (three acoustic modes) makes a relatively larger contribution to $\alpha^2F(\omega)$ than the others. λ (integration of $\lambda(\omega)$) characterizes the magnitude of correction of several physical properties due to the electron–phonon many-body interaction [32], such as quasi-particle energy, electronic heat capacity, effective mass, etc. Thus on the right of figure 8(a) we also show $\lambda(\omega)$ as a function of phonon frequency.

With equation (4), the calculated λ is 0.747, showing that the coupling strength between electrons and phonons in

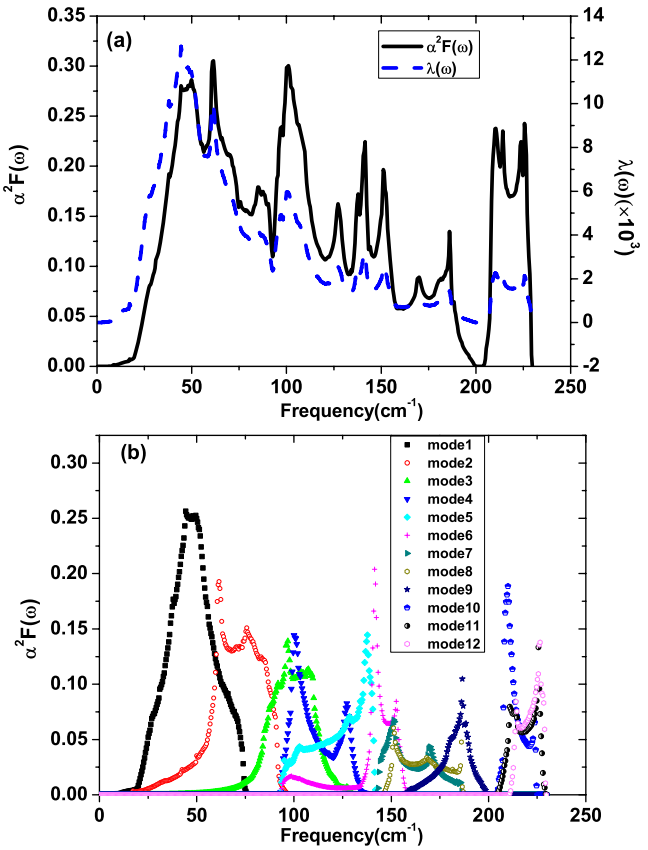

Figure 8. (a) The calculated Eliashberg function $\alpha^2F(\omega)$ and $\lambda(\omega)$ (see equation (4)); (b) phonon mode resolved Eliashberg function $\alpha^2F(\omega)$: mode-1 to mode-12 represent 12 phonon modes from low energy to high energy (see figure 6).

$ZrNi_2Ga$ is strong, and $\langle\omega\rangle_{\log}$ is found to be 68.48 cm^{-1} using equation (6). T_c is 3.15 K when choosing the screened Coulomb pseudopotential parameter μ^* to be 0.13 which lies in the typical range of approximated μ^*. The calculated T_c agrees well with 2.9 K [16] measured in previous experiments. For a clear understanding of the dependence of T_c on μ^*, we show additionally the curve of T_c versus μ^* in figure 9. It is found that T_c lies in the range of 3.99–2.62 K when μ^* is in the typical range 0.10–0.15. This further demonstrates that the superconducting behavior of $ZrNi_2Ga$ originates from electron–phonon coupling.

3.5. Thermodynamic properties

From the discussion above, we can conclude that in $ZrNi_2Ga$ phonon scattering of electrons plays a significant role in the transition from the normal state to the superconducting state. To have a more comprehensive insight into the influence of phonons exerted on $ZrNi_2Ga$, we investigate the contribution of phonons to its thermodynamics properties, assuming it is in the normal state. In figure 10, we show the phonon contribution to internal energy ΔE, Helmholtz free energy ΔF, constant-volume specific heat ΔC_v, along with entropy S, as a function of temperature in the framework of the harmonic

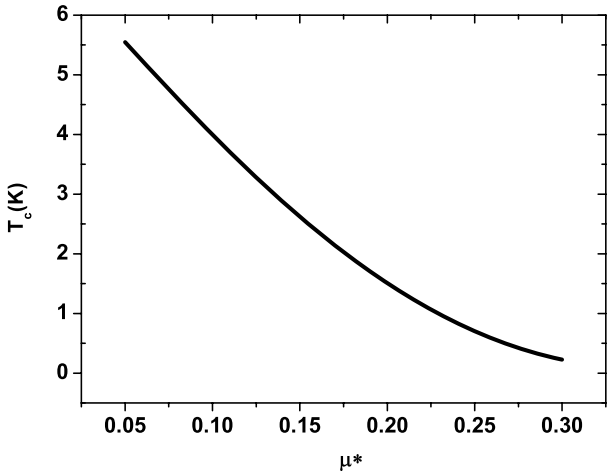

Figure 9. The superconducting transition temperature T_c as a function of the screened Coulomb pseudopotential parameter μ^*.

approximation. These quantities are defined as follows [33]:

$$\Delta E = \frac{3nN\hbar}{2}\int \omega \coth\left(\frac{\hbar\omega}{2k_BT}\right)g(\omega)\,d\omega \quad (7)$$

$$\Delta F = 3nNk_BT\int \ln\left\{2\sinh\left(\frac{\hbar\omega}{2k_BT}\right)\right\}g(\omega)\,d\omega \quad (8)$$

$$C_v = 3nNk_B\int \left(\frac{\hbar\omega}{2k_BT}\right)^2 \mathrm{csch}^2\left(\frac{\hbar\omega}{2k_BT}\right)g(\omega)\,d\omega \quad (9)$$

$$S = 3nNk_B\int\left[\frac{\hbar\omega}{2k_BT}\coth\left(\frac{\hbar\omega}{2k_BT}\right) - \ln\left\{2\sinh\left(\frac{\hbar\omega}{2k_BT}\right)\right\}\right]g(\omega)\,d\omega \quad (10)$$

where n is the number of atoms in the unit cell, N is the number of unit cells, $k_B = 1.38\times10^{-23}$ J K^{-1} and $g(\omega)$ is the PHDOS. The zero-point vibration is also taken into account such that ΔE and ΔF do not vanish at $T = 0$ K but both are 10.78 kJ mol^{-1}. ΔC_v increases rapidly in the low temperature region (below 100 K) and almost approach a constant in the high temperature region (above 200 K). Such behavior is in good agreement with that of ΔC_v stated in Debye specific heat theory, which points out that ΔC_v satisfies a T^3 law in the low temperature limit and that it is almost a constant $3nR$ in the high temperature limit, where $R = 8.314$ J mol^{-1} K^{-1} is the ideal gas constant. At 300 K, ΔC_v is already $11.446R$ which deviates a little from the high temperature limit of $12R$.

4. Summary

Using first-principles calculation, we investigate systematically the properties of $ZrNi_2Ga$ with an fcc $L2_1$ Heusler structure, including the electronic structure and phonon dispersion as well as the electron–phonon interaction and thermodynamics properties. For the electronic structure, the states around the Fermi energy are found to be dominated by Ni 3d-orbitals which are split by the combined crystal field from the Ga tetrahedron and Zr tetrahedron. The FSs resulting from three

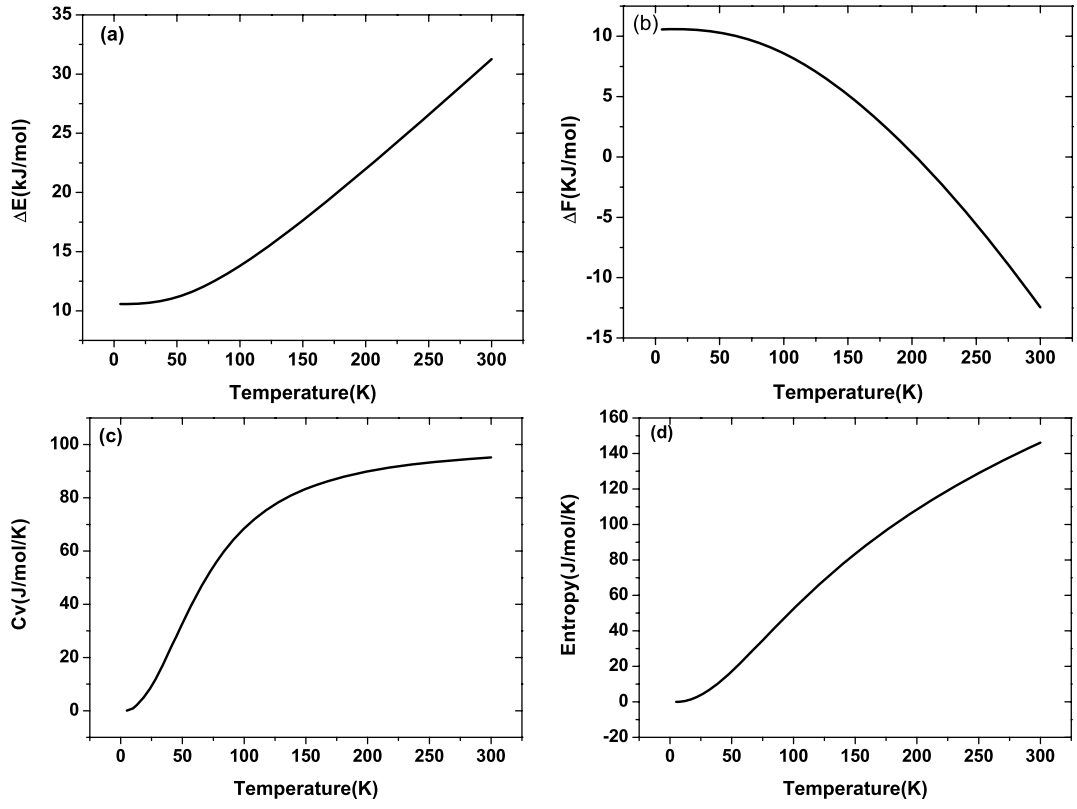

Figure 10. The calculated ΔE (a), ΔF (b), along with ΔC_v (c) and entropy S (d) as a function of temperature.

bands cutting across the Fermi energy are also shown. Phonon dispersion calculation shows that the optimized structure of $ZrNi_2Ga$ is in dynamic stability; Zr has strong vibration in the high energy region and the relatively low energy region is dominated by the vibration of Ni. Furthermore, $\alpha^2F(\omega)$ is obtained from electron–phonon interaction calculation. The deviation of the shape of $\alpha^2F(\omega)$ from that of PHDOS suggests that the phonons with lower energy (below 200 cm^{-1}) are more involved in the process of scattering of electrons than the phonons with higher energy. The calculated λ is 0.747, indicating the strong interaction between electron and phonon in $ZrNi_2Ga$. The estimated T_c from the Allen–Dynes formula is 3.15 K when choosing μ^* to be 0.13. This calculated T_c is in good agreement with the experimental counterpart. It means that $ZrNi_2Ga$ is a conventional phonon-mediated superconductor. In addition, the ΔE, ΔF, ΔC_v and S from the phonon contribution are also derived in the framework of the harmonic approximation.

Acknowledgments

We gratefully thank Guangtao Wang for his help and Professor Eyvaz Isaev for sharing the code calculating thermodynamic properties. This work is supported by the Natural Science Foundation of China (nos. 10674163 and 10534030), the MOST Project (nos. 2006CB921300 and 2007CB925000), and the Knowledge Innovation Project of the Chinese Academy of Sciences.

References

[1] Umetsu R, Kobayashi K, Fujita A, Oikawa K, Kainuma R and Ishida K 2005 *Phys. Rev.* B **72** 214412
[2] Block T, Carey M and Gurney B 2004 *Phys. Rev.* B **70** 205114
[3] Xie W, Xu Y and Liu B 2003 *Phys. Rev. Lett.* **91** 037204
[4] Zhao Y and Zunger A 2005 *Phys. Rev.* B **71** 132403
[5] Ishikawa M, Jorda J and Junod A 1982 *Superconductivity in d- and f-Band Metals* ed W Buckel and W Weber (Karlsruhe: Kernforschungszentrum) p 141
[6] Kierstead H, Dunlap B, Malik S, Umarji A and Shenoy G 1985 *Phys. Rev.* B **32** 135
[7] Shelton R, Hausermann-Berg L, Johnson M, Klavins P and Yang H 1986 *Phys. Rev.* B **34** 199
[8] Malik S, Umarji A and Shenoy G 1985 *Phys. Rev.* B **31** 6971
[9] Li W, Lynn J and Stanley H 1989 *Phys. Rev.* B **39** 4119
[10] Malik S, Umarji A and Shenoy G 1985 *Phys. Rev.* B **32** 4426
[11] Stanley H and Lynn J 1987 *J. Appl. Phys.* **61** 3371
[12] Wernick J, Hull G, Geballe T, Bernardini J and Waszczak J 1983 *Mater. Lett.* **2** 90
[13] Boff M, Fraga G, Brandão D and Gomes A 1996 *J. Magn. Magn. Mater.* **153** 135
[14] Waki S, Yamaguchi Y and Mitsugi K 1985 *J. Phys. Soc. Japan* **54** 1673
[15] Winterlik J, Fecher G and Felser C 2008 *Solid State Commun.* **145** 475
[16] Winterlik J, Fecher G and Felser C 2008 arXiv:cond-mat/08082356
[17] Kohn W and Sham L 1965 *Phys. Rev.* A **140** 1133
[18] Baroni S, de Gironcoli S and Dal Corso A 2001 *Rev. Mod. Phys.* **73** 515
[19] Blaha P *et al* 2001 *An Augmented Plane Wave + Local Orbitals Program for Calculating Crystal Properties* (K Schwarz, TU Wien, Austria)
[20] Blöchl P, Jepsen O and Andersen O 1994 *Phys. Rev.* B **49** 16223
[21] Baroni S *et al* http://www.quantum-espresso.org
[22] Rappe A, Rabe K, Kaxiras E and Joannopoulos J 1990 *Phys. Rev.* B **41** 1227
[23] http://opium.sourceforge.net
[24] Bauer R, Schmid A, Pavone P and Strauch D 1996 *Phys. Rev.* B **57** 11276
[25] Savrasov S and Savrasov D 1996 *Phys. Rev.* B **54** 16487
[26] Methfessel M and Paxton A 1989 *Phys. Rev.* B **40** 3616
[27] Murnaghan F 1944 *Proc. Natl Acad. Sci. USA* **30** 244
[28] Savrasov S, Savrasov D and Anderson O 1994 *Phys. Rev. Lett.* **72** 372
[29] Kong Y, Dolgov O, Jepsen O and Andersen O 2001 *Phys. Rev.* B **64** 020501(R)
[30] Allen P and Dynes R 1975 *Phys. Rev.* B **12** 905
Mcmillan W 1968 *Phys. Rev.* **167** 331
[31] Liu A, Mazin I and Kortus J 1994 *Phys. Rev. Lett.* **87** 087005
[32] Grimvall G 1981 *The Electron–Phonon Interaction in Metals* (Amsterdam: North-Holland)
[33] Maradudin A *et al* 1971 *Solid State Physics* 2nd edn (New York: Academic) chapter 4